ARTICLE IN PRESS
JID: OCEMOD [m5G;August 11, 2017;19:21]

Ocean Modelling 000 (2017) 1–14

Contents lists available at ScienceDirect

Ocean Modelling

journal homepage: www.elsevier.com/locate/ocemod

Virtual Special Issue
COWCLIP

Extreme waves in New Zealand waters

Victor A. Godoi[a,*], Karin R. Bryan[a], Scott A. Stephens[b], Richard M. Gorman[b]

[a] School of Science, University of Waikato, Hillcrest Rd, Hamilton, Waikato, New Zealand, 3216
[b] National Institute of Water and Atmospheric Research Ltd, Gate 10 Silverdale Rd, Hillcrest, Hamilton, Waikato, New Zealand, 3216

ARTICLE INFO

Article history:
Received 19 December 2016
Revised 27 July 2017
Accepted 3 August 2017
Available online xxx

Keywords:
Extreme waves
New Zealand
Wave climate
Climatic change
Continental shelf waters
Wave hindcasting

ABSTRACT

A detailed climatology of extreme wave events for New Zealand waters is presented, in addition to estimates of significant wave height (Hs) for up to a 100-year return period. Extreme events were explored using 44 years (1958–2001) of wave hindcast data. Comparisons to buoy data at three locations around New Zealand showed negative biases in the model, which nevertheless provided a suitable basis for trends, spatial distribution, and frequency analyses. Results indicate some similarities to patterns previously shown in the mean wave climate, with the largest waves found in southern New Zealand, and the smallest ones observed in areas sheltered from southwesterly swells. The number of extreme events varies substantially throughout the year, while the differences in intensity are more consistent. Events occur more/less frequently in winter/summer months. The greatest mean annual variability of extreme Hs is found on the north coasts of both the North and South Islands, where more locally-generated storms drive the extremes. The interannual variability is largest along the north coast of the country and on the east coast of the South Island, suggesting relationships with La Niña-like effects and the Southern Annular Mode, respectively, which past work showed to be important drivers in these regions. Moreover, the known trend for a more positive Southern Annular Mode may explain the increasing number of extreme events shown in our study.

1. Introduction

Extreme wave events have been recognised as a major issue for safety in both coastal and offshore regions. With the ongoing concerns about changes in the frequency and magnitude of cyclones across the globe (Simmonds and Keay, 2000), and the high vulnerability of coastal areas to wave attack as the sea level rises (Hannah, 2004; Hannah and Bell, 2012; Hauer et al., 2016), there is a need to understand and predict the behaviour of extreme wave events.

Climatologies have generally been established for the mean state of the ocean, whereas the equivalent for extreme events is not as common despite the valuable information that these can provide for the management of coastal erosion and flooding (Horrillo-Caraballo et al., 2012), for example. One impediment to examining extreme values is that the different statistical characteristics of extreme and non-extreme wave events (Young et al., 2012) require them to be analysed separately.

One of the most common ways to assess extreme wave events is to calculate return-period values for significant wave height (Hs) (e.g., Alves and Young 2003; Guedes Soares and Scotto, 2004). The 100-year return value of Hs, for example, is the Hs value exceeded, on average, once in 100 years (Carter and Draper, 1988). Such values are required for engineering design because extreme waves can have major impacts on safety, operability of shipping and structures, and the economics of offshore facilities (Young et al., 2012). Several studies have estimated return values of Hs on a global spatial scale using modelled results (e.g., Caires and Sterl, 2005), satellite altimetry data (e.g., Izaguirre et al., 2011; Vinoth and Young, 2011; Young et al., 2012) and buoy measurements (e.g., Hemer, 2010). However, global models and satellite measurements do not generally provide sufficiently high-resolution data for predicting return values precisely near coastal areas. Although many local studies have been conducted for specific areas (e.g., the Portuguese coast (Ferreira and Guedes Soares, 1998), the Persian Gulf (Moeini et al., 2010), the Australian region (Hemer et al., 2016), and the Kuwaiti waters (Neelamani et al., 2007)), several regions in

* Corresponding author.
E-mail addresses: victorgodoirj@gmail.com (V.A. Godoi), karin.bryan@waikato.ac.nz (K.R. Bryan), scott.stephens@niwa.co.nz (S.A. Stephens), richard.gorman@niwa.co.nz (R.M. Gorman).

http://dx.doi.org/10.1016/j.ocemod.2017.08.004

Please cite this article as: V.A. Godoi et al., Extreme waves in New Zealand waters, Ocean Modelling (2017), http://dx.doi.org/10.1016/j.ocemod.2017.08.004

the world still lack investigation, especially in the Southern Hemisphere (e.g., New Zealand).

The international interest in the water bodies surrounding New Zealand has grown with the implementation of various trade agreements (World Bank Group, 2016), which increase traffic along key shipping routes, and with the recognised importance of the Southern Ocean in regulating the Earth's climate (Lavergne et al., 2014). New Zealand is an island nation highly influenced by its surrounding oceans. The country lies at the mid-latitudes of the Southern Hemisphere and is affected by a range of atmospheric systems. Large waves, generated by extratropical cyclones, propagate without major obstacles through the Southern Ocean, and affect a large portion of the New Zealand coastline (Godoi et al., 2016; Gorman et al., 2003a, 2003b). Additionally, waves formed by tropical cyclones also play a significant role, especially on the north coast. A recent study (Godoi et al., 2016) showed the influence of climatic patterns on the average wave climate around New Zealand in addition to an increasing trend in Hs along the coast. New Zealand's coastal population has been growing in the last decades (Bryan et al., 2008), and therefore, improved predictions for coastal planning are required to deal with the threat posed by extreme wave events in this complex environment.

The paucity of wave data around New Zealand has made it difficult to accurately provide an extreme wave climatology (synthesis of extreme wave conditions based on long-term statistics) and conduct extreme wave predictions (Stephens and Gorman, 2006). Buoy measurements are generally taken as ground truth (e.g., Hemer, 2010). However, short duration records and insufficient number of buoys preclude reliable estimates of return values in many cases. Satellite altimetry data can also be problematic; among the drawbacks is the temporal coverage of measurements: the infrequent revisit (typically 10 days) of the satellite to a particular location makes it difficult to adequately capture storm peaks. Stephens and Gorman (2006) conducted an extreme wave analysis for six sites off the New Zealand coast by using results from a 20-year hindcast, providing evidence of the importance of modelled results when a long dataset is required.

The accuracy of extreme predictions depends on the accuracy and length of input data (Stephens and Gorman, 2006). Using results from the 45-year (September 1957–August 2002) high resolution wave hindcast (hereafter 45WH), conducted by Gorman et al. (2010), we have created an extreme wave climatology for the New Zealand continental shelf waters, and analysed trends and patterns in extreme events. In order to complement our study, the extreme estimates carried out by Stephens and Gorman (2006) have been extended to shallower waters. The 45WH covers a considerably longer time period than the hindcast used by Stephens and Gorman (2006) and has higher space-time resolution in shallow waters, which make the new modelled data more suitable for predicting extreme events and establishing an extreme wave climatology.

2. Dataset

In order to conduct the extreme wave analysis, modelled time series of Hs and mean wave period (Tm-10, hereafter Tmean) were extracted from the regional grid domain (Fig. 1) of the 45WH. Tmean was chosen over the peak wave period (Tpeak) because the latter was sometimes undefined in the hindcast data because of missing values close to the shore. As Tm-10 is more weighted to lower frequencies than Tm-01 and Tm-02, it is more representative of swell, and so a better proxy for Tpeak. Only the full calendar years (1958–2001) of the 45WH have been used. The 45WH was conducted using the WAVEWATCH III v. 3.14 model (Tolman, 2009) forced with 1.125° spatial resolution wind and ice fields from the ERA-40 reanalysis project (Uppala et al., 2005) on a global grid at $1.125^\circ \times 1.125^\circ$ resolution. One-way nested within the global grid, a regional grid domain, with $0.125^\circ \times 0.09375^\circ$ (approximately 10 km) resolution, encompassed part of the Tasman Sea and parts of the Southern and southwestern Pacific oceans. The regional grid provided a higher-resolution representation of nearshore wave processes, although the same ERA-40 inputs were used as for the global simulation. Mean wave parameters were output at 1 h and 3 h intervals for the regional and global domains, respectively. These have been validated against buoy measurements, located mainly around New Zealand and North America, and satellite altimetry data, obtained from the TOPEX/Poseidon, ERS1 and ERS2 missions. A mean root-mean-square error of 0.50 m and mean correlation of 0.83 were obtained from comparisons of Hs between the regional results and New Zealand buoy data (Godoi et al., 2016; Gorman et al., 2010). Comparisons to altimeter data over the regional hindcast area show positive bias in Hs, of up to +0.3 m, in offshore waters of the Tasman Sea and Southern Ocean, and negative bias near the coast, of down to −0.3 m. The spatial pattern of bias is similar to the results of Chawla et al. (2013). Additional details of the model simulation and its validation can be found in Gorman et al. (2010) and Godoi et al. (2016).

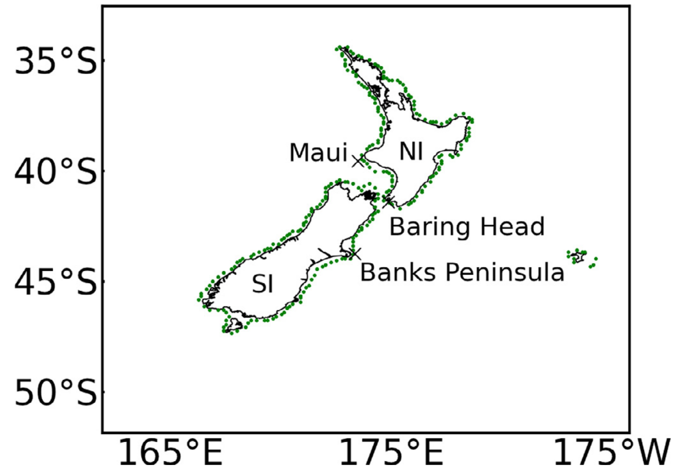

Fig. 1. Regional grid domain of the 45-year wave hindcast. Green dots represent the model grid points on the 50 m isobath, whereas crosses indicate the buoy locations. NI and SI stand for North Island and South Island, respectively. (For interpretation of the references to colour in this figure legend, the reader is referred to the web version of this article.)

Large waves were generally underestimated by the model in comparison to buoy measurements (Gorman et al., 2010). This is consistent with the triple-collocation study of Caires and Sterl (2003), who showed that ERA-40 tended to underpredict high wind speeds compared to ERS-1 and TOPEX measurements, while the wave model correspondingly underpredicted the upper range of significant wave heights from buoy and altimeter records. The underestimation of large waves in the 45WH may have arisen from two factors. The first is the relatively low space-time resolution of the ERA-40 winds, which does not take abrupt changes in direction and substantial wind speed gradients into account (Godoi et al., 2016); and the second is the use of the formulation proposed by Tolman and Chalikov (1996) in the hindcast, which underestimates the energy input during intense storm conditions dominated by young wind-sea (Ardhuin et al., 2007). Uppala et al. (2005) observed that the detection of tropical cyclones in the Southern Hemisphere exceeded 90% in comparison to a best-track dataset (Neumann, 1993) for the period from 1973 onwards. However, the percentages of detection in ERA-40 for the periods 1958–66 and 1967–72 were 75% and 82%, respectively. Furthermore, ERA-40 tends to underestimate wind speeds above 14 m/s (Caires et al., 2004). Regarding the second factor, Stopa et al. (2016) compared

Table 1
Buoy deployments. NIWA stands for National Institute of Water and Atmospheric Research Ltd.

Site	Longitude (°)	Latitude (°)	Recording period	Source
Baring Head	174.8467	−41.4022	03 Aug 1998–19 Dec 2013	NIWA
Banks Peninsula	173.3348	−43.7558	06 Feb 1999–28 Feb 2014	NIWA
Maui	173.45	−39.55	31 Aug 1976–30 Apr 1987	Shell, BP, Todd University of Auckland

the performance of various sets of parameterisations for the same wind input. The ST4 parameterisation (Ardhuin et al., 2010) did best across the Hs range, while ST2 (Tolman and Chalikov, 1996) had high positive bias in the lower range, decreasing for larger wave heights. This seems consistent with insufficient swell dissipation and underestimation of wind-sea, in ST2. It also shows that while ST4 is a better choice now that it is available, the deficiencies of ST2 are not as significant for extreme climate as for mean climate. In order to determine properly the individual contributions of the wind fields and the set of parameterisations used in the present work to the underestimation of extreme waves, a set of tests would be required. These include doing several model runs using the same set of parameterisations combined with wind fields from different sources (not only ERA-40), as well as testing different sets of parameterisations forced with ERA-40 wind fields (similar to what was done by Stopa et al. (2016)). Then, the results should be compared to observed data. Another way of validating a specific set of parameterisations is to test them against other sets that have been validated already. Conducting these tests is beyond the scope of the paper.

Although the underestimation of large waves is acknowledged, the lack of long buoy records to account for extreme events in the study region forced the use of uncalibrated modelled data in our study. A possible solution for calibrating the model data would have been estimating an approximate bias for extreme Hs from comparisons between model and buoy data. However, implementing this solution in shallow waters based on just a few buoy records is likely to lead to erroneous calibration, especially when land-sheltering effects prevail due to buoy proximity to the coast and headlands. As a consequence of these effects in addition to short buoy records, the bias varies considerably around the coast, and so would have caused spurious calibrations (as shown by Stephens and Gorman (2006)). Despite the recognised underprediction of extreme events by the model, its results still allowed exploration of the spatial distribution of extreme events, their trends and clustering patterns. Although a calibration procedure was not performed, model and buoy data were compared in terms of the probability of occurrence of extremes at the locations where buoy data do exist and span more than 10 years (Fig. 1).

Buoy records from twelve sites around New Zealand were analysed regarding their suitability for extreme wave predictions (not shown), and only three of them (Table 1, Fig. 1) were considered to be of sufficiently long duration. The others were short records due to either short recording periods or large gaps of missing data after spike removal, hence they will not be discussed further. Thus, Hs time series were extracted from the buoy and model data at the coordinates shown in Table 1.

Besides the Hs time series extracted at the buoy sites, two additional datasets from the model data have been used to assess extreme events, the annual maxima Hs and Peaks-Over-Threshold (POT) data. The latter are defined here as maxima Hs from independent storms, with maxima Hs being considered only if above the 99th percentile (of the full hourly dataset) and separated by a minimum interval of 72 h. The set of maxima of Hs identified by the POT approach and the annual maxima Hs are also referred to as "extreme Hs". Due to computational costs, POT data have been produced only at 247 model grid points on the 50 m isobath around New Zealand (Fig. 1).

3. Extreme wave climatology

Monthly and seasonal climatologies of extreme events over the 44-year (1958–2001) period were defined using the POT dataset on the 50 m isobath. Averages of extreme Hs and number of extreme wave events were computed for the 12 months and 4 seasons over all years (summer: Dec, Jan, Feb; autumn: Mar, Apr, May; winter: Jun, Jul, Aug; spring: Sep, Oct, Nov). The mean annual and interannual variabilities (MAV and IAV, respectively) of extreme Hs were also calculated. The MAV of extreme Hs was computed by normalizing the average of the annual standard deviation of extreme Hs by the annual average of extreme Hs, while the IAV was determined by the standard deviation of the annual means of extreme Hs normalized by the overall mean of extreme Hs (Godoi et al., 2016; Stopa et al., 2013). Lastly, monotonic trends in the values of extreme Hs and in the number of extreme events were evaluated using the Mann–Kendall test (Mann, 1945; Kendall, 1955). The magnitude of the trends was computed by employing the Theil–Sen estimator (Theil, 1950; Sen, 1968). Annual average extreme Hs (using POT data) and annual maxima Hs were used to calculate height trends, whilst number trends were computed using time series of the annual number of extreme Hs peaks (calculated using the POT data).

Fig. 2 shows the 44-year (1958–2001) mean annual maxima Hs and its corresponding Tmean (44-year mean annual Tmean associated with annual maxima Hs), providing an overview of different extreme wave climates around New Zealand. The spatial pattern of mean annual maxima Hs (Fig. 2a) closely resembles the mean wave climate (Godoi et al., 2016; Laing, 2000; Pickrill and Mitchell, 1979), in which the roughest seas occur in southern New Zealand, associated with largest Tmean (Fig. 2b), and calmer conditions occur in regions sheltered from southwesterly swells. Such swells are obstructed by the landmass, creating a distinctive shadow zone and relatively smaller Tmean to the north of the country (Fig. 2b). The largest waves on the north coast are generally associated with tropical cyclones (Gorman et al., 2003a), and are considerably less frequent than the steady swells, originated by extratropical cyclones, that hit most other parts of the New Zealand coastline.

A cluster analysis was performed to thoroughly characterise extreme wave climates around the country (Fig. 3) by using the 44-year mean annual maxima Hs (44Hs) and its corresponding Tmean (44Tmean) (standardised to a Gaussian distribution – zero mean and unit variance) and the *k*-means algorithm (Hartigan and Wong, 1979; Kanungo et al., 2002). The cluster analysis jointly examines the input parameters and distinguishes clusters by grouping data with similar characteristics. Each colour of Fig. 3 represents one cluster, in which all grid points within can be thought as having a similar wave climate. The red cluster (spatial averages of 44Hs and 44Tmean equal to 8.94 m and 12.09 s, respectively – Fig. 3a) represents areas dominated by large swells originated in the Southern Ocean. A shadow zone appears as soon as the propagation of these swells begins to be interrupted by the New Zealand landmass (grey cluster – spatial averages of 44Hs and 44Tmean equal to 7.18 m and 11.11 s, respectively – Fig. 3a). Further sheltering, associated with a lower-energy wave climate (orange cluster - spatial averages of 44Hs and 44Tmean equal to 5.97 m and 9.87 s, respectively – Fig. 3a), is observed in the regions affected by a more pronounced refraction of southwesterly swells (on the east and west

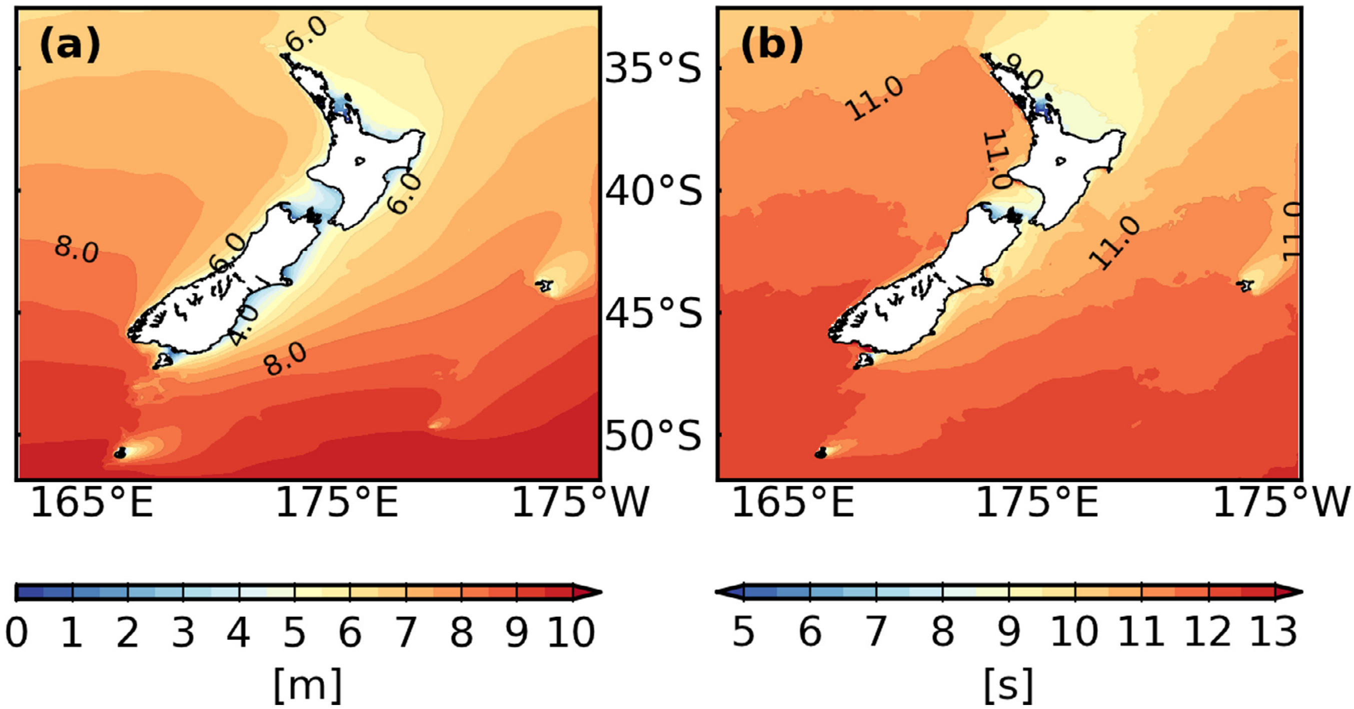

Fig. 2. Forty-four year (1958–2001) mean (a) annual maxima significant wave height; (b) mean wave period associated with annual maxima significant wave height.

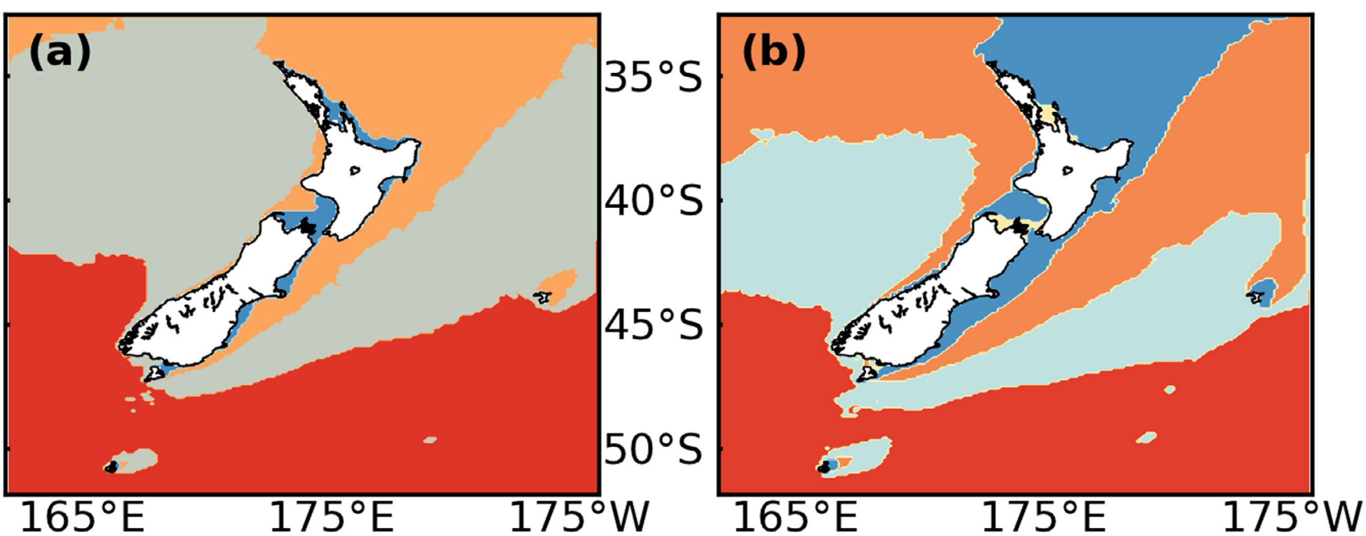

Fig. 3. Cluster analysis results using 44-year (1958–2001) averages of annual maxima Hs and corresponding mean wave periods (a) 4 clusters; (b) 5 clusters. Each colour represents one cluster. (For interpretation of the references to colour in this figure legend, the reader is referred to the web version of this article.)

coasts), or where they are blocked by the landmass (to the north of the northern coast). The most sheltered zone, dominated by low (or infrequent large) swells and local wind-sea waves, is represented by the blue cluster (spatial averages of 44Hs and 44Tmean equal to 2.69 m and 8.18 s, respectively – Fig. 3a). The five clusters in Fig. 3b provide similar information, but also show an additional low-energy wind-sea-wave-dominated environment in sheltered embayed areas (yellow cluster - spatial averages of 44Hs and 44Tmean equal to 1.88 m and 6.94 s, respectively). The patterns described can also be observed in Fig. 2a. Taking into account both the cluster analysis results (Fig. 3) and the long-term means (Fig. 2), as well as the wave climate classification by Pickrill and Mitchell (1979) and Godoi et al. (2016), we divide the regions immediately adjacent to the coastline into four main extreme wave climates. These are basically demarcated by the coastline orientation, and can be roughly related to the four cardinal directions (north, east, south, and west). Thus, the analyses have been conducted focusing on these four main wave climates.

The annual average of extreme wave events was calculated at the model grid points on the 50 m isobath using POT data (Fig. 4). Its values varied in the range of 2.8–6.4 events per year in the period 1958–2001, with the highest values found in the region between the two main islands of New Zealand. A large number of events also took place on the northeastern part of the country and on the central western coast of the South Island, meaning that extreme events were more closely-spaced in these regions. The frequency of extreme events is highly dependent on the time of the year (shown next) and coastline exposure to generating regions.

Monthly climatologies of extreme wave events (magnitude of Hs and number of events) calculated using the POT data can be

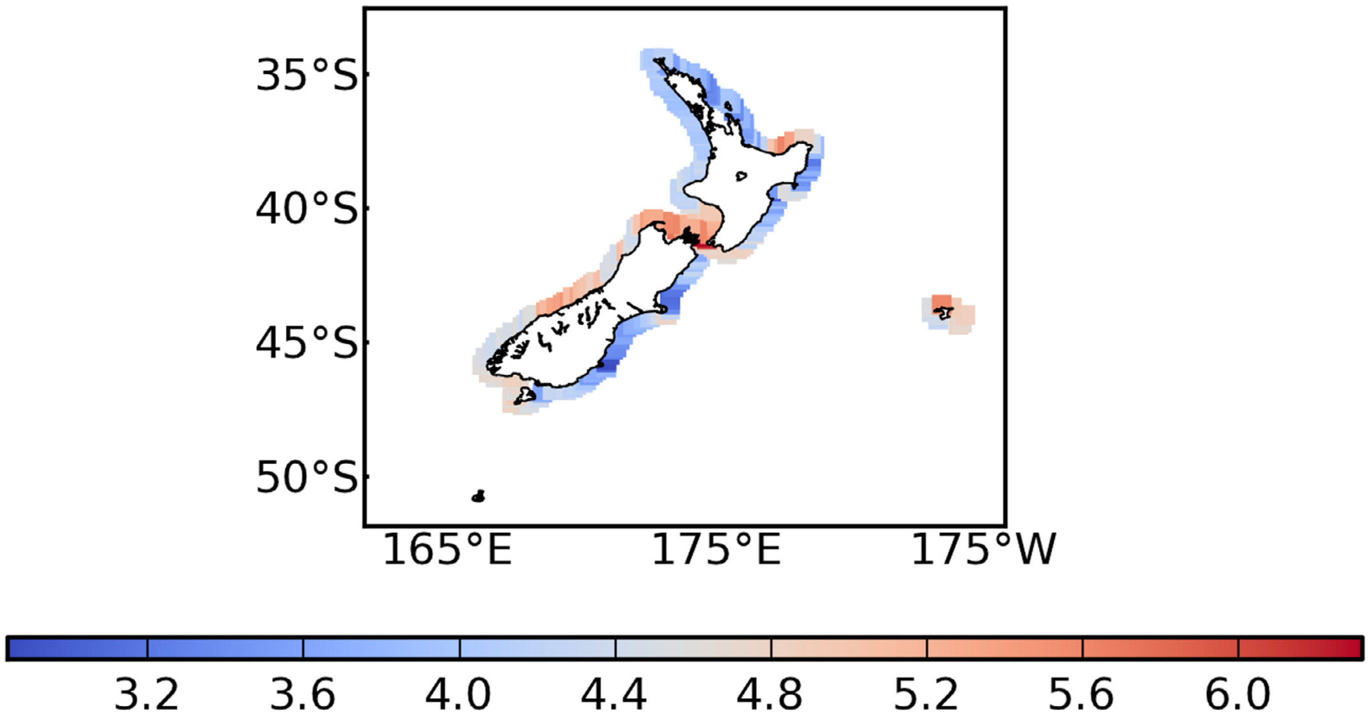

Fig. 4. Annual average number of extreme wave events at the model grid points on the 50 m isobath (calculated using POT data).

found in Figs. 5 and 6. The southwestern and southern coasts received the most energetic waves followed by the northwestern coast. This can be associated with extratropical cyclones generated by the westerly air flow in mid-latitudes, which produce large wave events in all months. The southernmost region of the North Island also showed intense extreme wave activity throughout all months, which can be associated with southerly swells. The mildest extreme waves were generally found in the sheltered strait between the North and South islands, where southwesterly swells are blocked by the landmass. There was little variation throughout the seasons in the spatial pattern of extreme Hs (not shown). Despite that, 47% of the examined sites received the largest waves in winter, 33% in autumn, 11% in summer, and 9% in spring. There was a remarkable contrast in the frequency of extreme wave events between the summer and winter months (Fig. 6). Essentially the whole country was affected by a great number of closely-spaced extreme Hs in winter time, whereas the opposite was true for summer. In fact, the highest frequency of events on the west and south coasts occurred in May (an autumn month), while on the east and north coasts it prevailed in June and July, respectively. The frequency was also high in most parts of the coastline in August. On the other hand, extreme events were least frequent in January and February. Although the wave intensity did not change considerably throughout the year, extreme events were more commonly observed from May to August. This means that there is a higher chance of erosion due to sequences of storms during those months, as well as a higher chance of extreme events coincide with a high tide, leading to multi-hazard effects.

Like the MAV of mean Hs (Godoi et al., 2016), the MAV of extreme Hs was greatest in regions sheltered from southerly swells, emphasising the role played by locally-generated storms (Fig. 7a). Extreme waves generated by tropical cyclones propagating to the north of New Zealand hit the north coast, especially in summer (Gorman et al., 2003a), contributing to the large variability in the region. The largest IAV (Fig. 7b) was found in the central north coast, denoting a relationship with La Niña-like effects (stronger northeasterly winds to the north of New Zealand). The east coast of the South Island had also relatively large IAV, which might be related to the Southern Annular Mode (SAM). Positive phases of the SAM result in strengthened westerly winds in the Southern Ocean (Kushner et al., 2001; Marshall, 2003), and a trend toward its positive phase has been detected since the mid-1960s (Marshall, 2003).

Trends in extreme Hs calculated from both annual maxima Hs (Fig. 8a) and the annual average extreme Hs (computed using the POT data) (Fig. 8b) showed some similarities regarding the spatial distribution along the coast. Notwithstanding, the ranges of magnitude of their trends presented notable distinction, varying from −2.09 to 3.43 cm/yr in the first (Fig. 8a) and from −0.96 to 0.91 cm/yr in the second (Fig. 8b). Only statistically significant trends at the 95% confidence level are displayed. There was no statistically significant trend in extreme Hs at most locations around the New Zealand coast. Increasing extreme Hs occurred on the northeastern part of the South Island, while a negative trend was observed in part of the west coast of the South Island in both datasets. Notable increasing trends in annual maxima Hs were also detected on the southeastern coast (Fig. 8a). Such trends and the increasing extreme Hs observed on the northeastern coast of the South Island are consistent with the positive trend in the SAM, which has led to the strengthening of the westerly winds in the Southern Ocean (Gillett and Thompson, 2003; Hemer, 2010; Marshall, 2003; Schott et al., 2009). Stronger westerly winds generate more intense extratropical cyclones, which also justify the positive trends in the number of extreme events on the south and east coasts (Fig. 8c). These trends indicate that extreme events became more frequent over the 44 years (1958–2001) analysed. Quantitatively, 33.60% of the POT data showed positive trends in the annual number of extreme events, 65.59% presented no statistically significant trends, and only 0.81% showed negative trends. Regarding the trends in the annual average extreme Hs, 2.02% of the sites on the 50 m isobath had positive trends, whilst 6.48% had negative trends. Only increasing wave heights, varying mostly in the range of 1–6 cm/decade along the New Zealand coastline, were documented by Godoi et al. (2016) when the mean of the whole spectrum of waves was analysed. This supports the idea that ex-

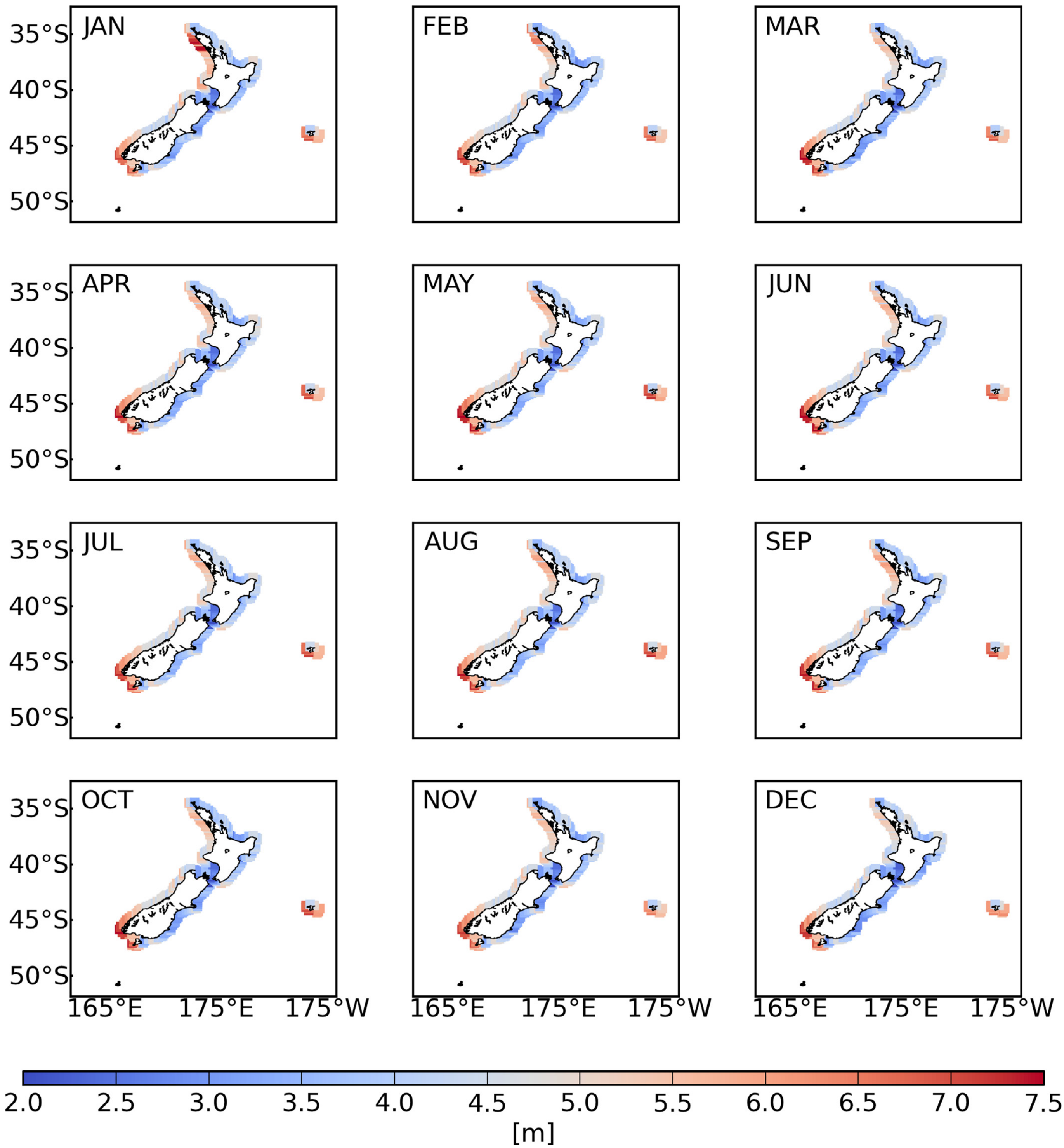

Fig. 5. Monthly climatology of extreme Hs calculated using POT data on the 50 m isobath.

treme and mean wave conditions should be treated separately, like in Ruggiero et al. (2010).

4. Extreme value analysis

Extreme value theory has been widely used for estimating return values from Hs datasets (e.g., Caires and Sterl, 2005; Hemer, 2010; Izaguirre et al., 2011; Méndez et al., 2006, 2008; Menéndez et al., 2009; Vinoth and Young, 2011). Although several methodologies are available, there is no universal approach that is suitable for all datasets. However, there are two commonly-accepted methods in general use: the generalised extreme value (GEV) model fitted to annual maxima (AM), and the generalised Pareto distribution (GPD) fitted to peaks-over-threshold (POT) (Coles, 2001). The reader is referred to the following literature for details of extreme value theory and the limitations and advantages of each method, Caires and Sterl (2005), Coles (2001), Ferreira and Guedes Soares (1998), Holthuijsen (2007), Mathiesen et al. (1994), Stephens and Gorman (2006), Vinoth and Young (2011), and Young et al. (2012).

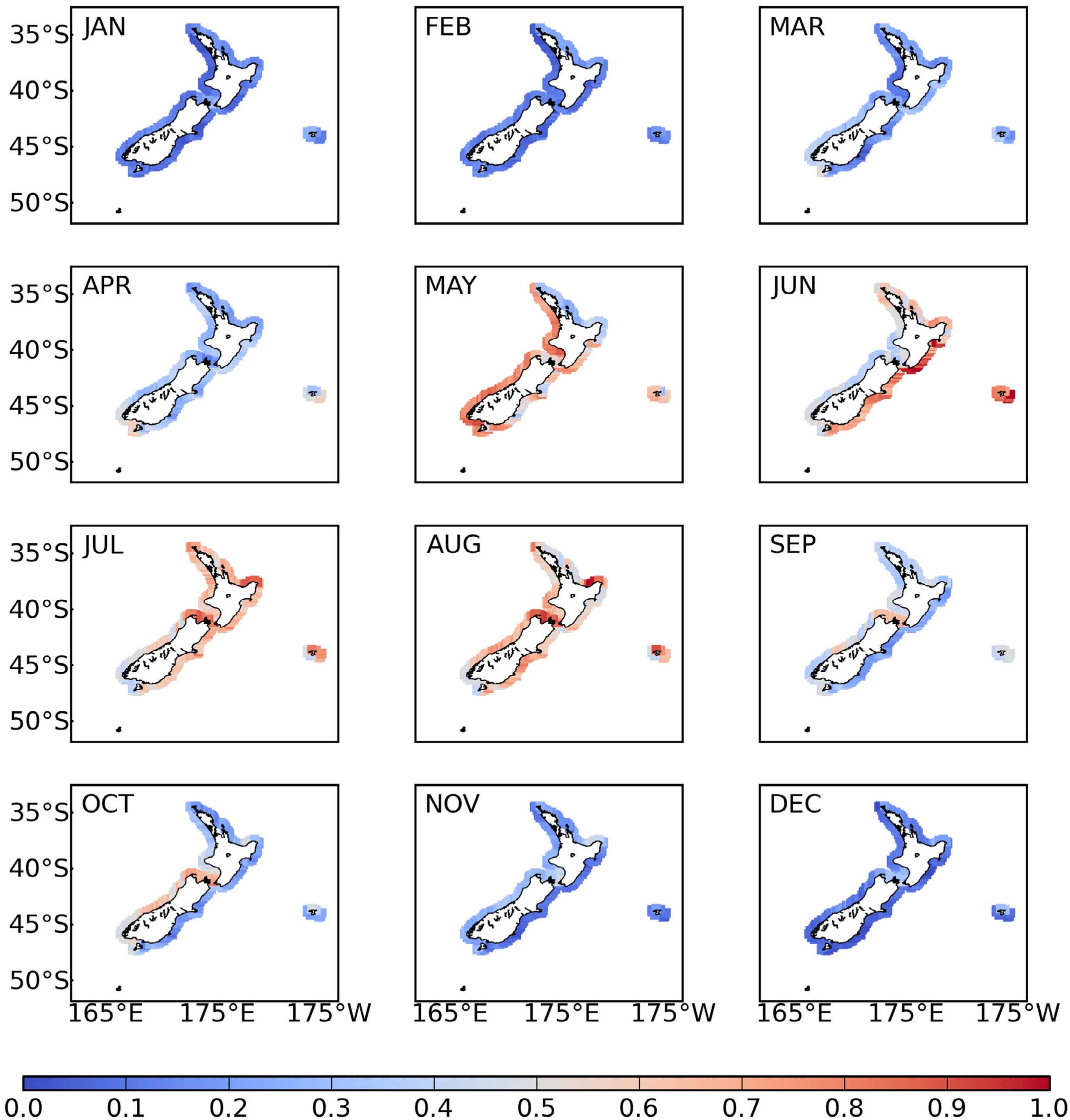

Fig. 6. Monthly climatology of the number of extreme wave events calculated using POT data on the 50 m isobath.

The main drawbacks of the two aforementioned techniques are that the AM-GEV method requires long datasets to provide satisfactory estimates, not being practical for many oceanographic purposes (Young et al., 2012), whereas the POT-GPD method needs arbitrary thresholds to be established, which can be problematic in certain circumstances (e.g., Mazas and Hamm, 2011). Considering the 45-year wave hindcast available, both methods seem to be reasonable candidates, hence they have been adopted here. In the case of the POT approach, a long dataset allows us to choose a high threshold in order to avoid its underestimation and ensure satisfactory fitting of the model cumulative distribution function (CDF) to the empirical CDF. One should ideally select the lowest threshold at which the GPD is valid, because higher thresholds generate fewer peaks with which the GPD parameters can be estimated, hence reducing the confidence in the return values (Caires and Sterl, 2005; Coles, 2001). The selected threshold (discussed below) provided about 3–6 Hs peaks per year at the 247 sites along the 50 m isobath, which is a typical number for extreme value analyses of environmental variables (e.g., Coles, 2001).

The use of percentiles to select thresholds is a common practice when dealing with several geographical locations and sufficiently long datasets. Different percentiles have been used

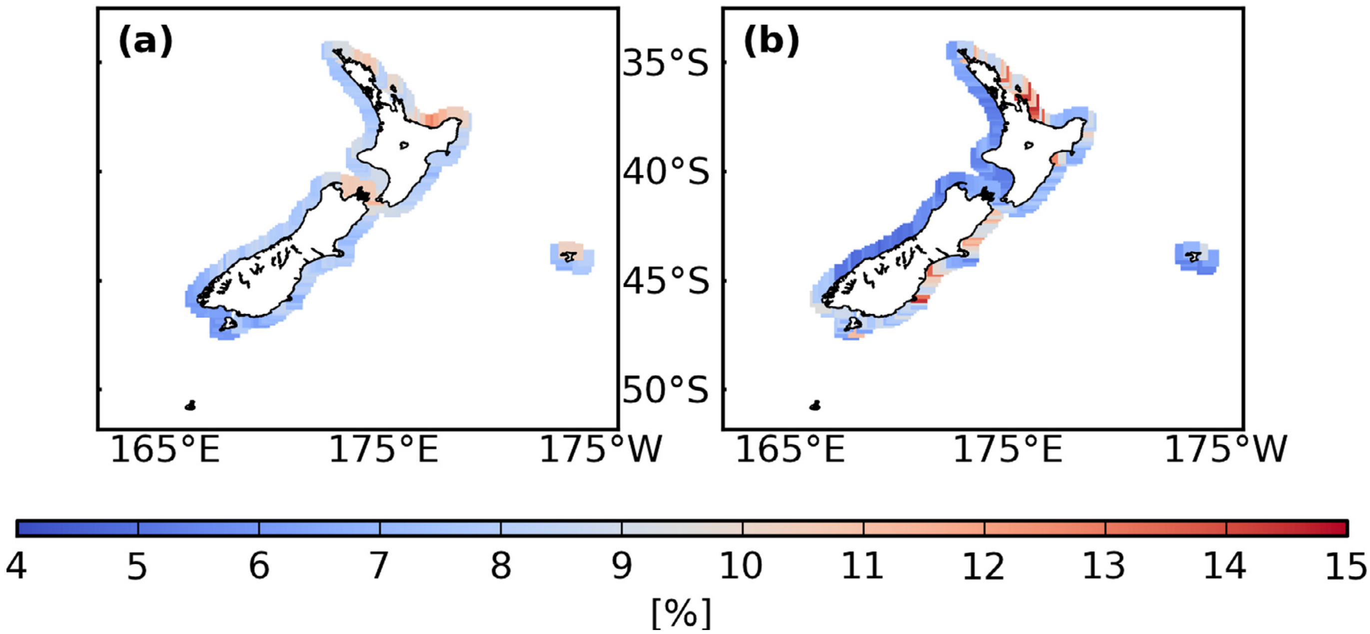

Fig. 7. (a) Mean annual variability of extreme Hs; (b) Interannual variability of extreme Hs. Both statistics were calculated using POT data on the 50 m isobath.

in the literature, for example, the 90th and 97th used by Caires and Sterl (2005), the 90th and 93rd adopted by Vinoth and Young (2011), and the 99.5th used by Méndez et al. (2008). Here, the 99th percentile was selected to identify extreme events using the POT approach. As specified in Section 2, the POT data are defined as maxima Hs (above the 99th percentile) from independent storms separated by a minimum interval of 72 h. The 72-h interval ensures independence between events, and was based on previous work, such as Alves and Young (2003), Méndez et al. (2006, 2008), and Stephens and Gorman (2006). Shorter intervals have also been chosen in the literature, as for instance, the 48-h interval considered by Harley et al. (2010) and Swail et al. (2006). The extreme value theory requires identical distribution of observations, which implies that waves generated by different atmospheric sources (e.g., cyclone, anticyclone, and trade winds) should be treated separately (Vinoth and Young, 2011). Given the number of sites and the relatively long period involved in the present analysis, it was not possible to meet the identical distribution criterion (also the case in other studies, such as Alves and Young (2003) and Stephens and Gorman (2006)). Nevertheless, the coastline orientation facilitates, to a certain extent, that waves generated by different atmospheric sources be separated into different populations, since weather systems affect some coasts more than others.

Finally, Hs return values were estimated for return periods of up to 100 years in the whole regional grid domain using the AM-GEV technique, and at the model grid points on the 50 m isobath using the POT-GPD approach. Both extreme models (GEV and GPD) were fitted to extreme Hs (annual maxima and POT data, respectively) employing the maximum likelihood method.

Very similar 100-year Hs return values were estimated by the two methods at the model grid points on the 50 m isobath (Fig. 9). Their estimates were compared using two statistical metrics, the Pearson's correlation coefficient (R) and root-mean-square error ($RMSE$). Although the largest return values were slightly overestimated by the AM-GEV method in comparison to the POT-GPD method, shown by the deviation of the points from the line of equivalence (1:1) at highest quantiles (Fig. 9), a high degree of correlation was found ($R = 0.99$) in addition to a relatively low $RMSE$ ($RMSE = 0.17$), meaning satisfactory agreement between the two datasets. Thus, the 100-year Hs return value estimates calculated at the model grid points along the 50 m isobath are shown only for the POT-GPD method (Fig. 10a). The largest waves were estimated on the southwestern coast, followed by the west coast of the North Island. The southern and northeastern parts of the North Island also showed large wave estimates. On the other hand, the lowest estimates were obtained near the coastlines surrounding the strait between the two main islands (Cook Strait). The spatial pattern shown by the 100-year return values is similar to that found for the mean conditions, as seen in Godoi et al. (2016). Given the satisfactory agreement between both approaches for different wave climates along the 50 m isobath, it is expected that the other model grid points of the regional domain behave likewise. Thus, 100-year Hs return values were estimated for the whole regional domain using only the AM-GEV approach (Fig. 10b).

The spatial distribution of Hs return values (Fig. 10b) again showed similar patterns to the mean Hs (Godoi et al., 2016), in which the smallest waves are seen in regions sheltered from southwesterly swells, and the largest ones are observed south of New Zealand. Stephens and Gorman (2006) obtained the same result, but also reported smaller spatial variation compared to the spatial variation in the average waves. We estimated lower 100-year Hs return values than Stephens and Gorman (2006), with the difference being even greater to the south of New Zealand. Although uncalibrated modelled data have been used in both studies, it is important to highlight the considerably higher space-time resolution and longer record (more than twice as long) employed in the present analysis, both relevant characteristics for satisfactory return value estimation. Stephens and Gorman (2006) also used a different extreme value method (Mathiesen et al., 1994), which has since been superseded in general practice by the methods used here. However, it is also worth emphasising that an underprediction by the model relative to buoy measurements is still present.

Three locations (Fig. 1), where buoy records span more than 10 years, have been selected in order to compare Hs return values estimated from both the model and buoy data (Fig. 12). Due to the lengths of the buoy records being relatively short (<16 years), the AM-GEV approach was disregarded, and only the POT-GPD method has been implemented. As the buoy records are not as long as the model time series, the threshold selection was initially based on the assessment of the stability of the shape and scale parame-

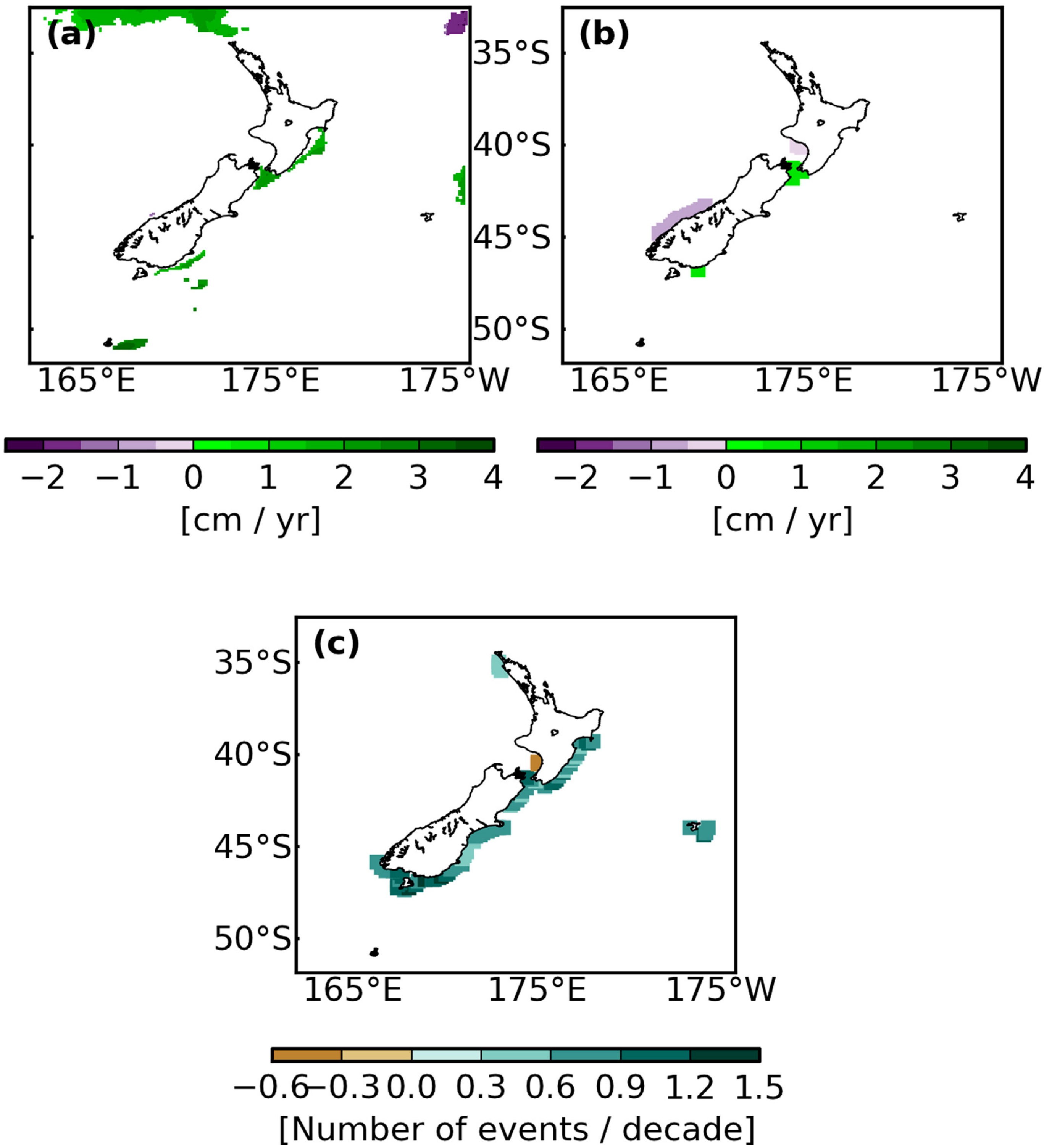

Fig. 8. Monotonic trends in (a) annual maxima Hs; (b) the annual average extreme Hs; (c) the number of extreme wave events. Trends in (a) were computed for the whole regional domain of the 45-year wave hindcast, whereas in (b) and (c) they were calculated using POT data on the 50 m isobath. Only statistically significant values at the 95% confidence level were plotted. Significance was computed using *p*-value.

ters obtained from the fitting of the GPD across a range of different thresholds, as demonstrated in Coles (2001). Nevertheless, this methodology provided almost identical return value estimates to when thresholds were selected based on the 99th percentile of the time series (not shown). Thus, the latter has been adopted in order to follow the same procedures applied to the model data. Before estimating Hs return values from the buoy and model data at the buoy sites, a validation of the matching peaks between these two datasets was carried out for overlapping periods (Fig. 11). Again, the selection of Hs storm peaks was made based on the 99th percentile threshold of the whole time series and on a minimum interval of 72 h between consecutive peaks. In general, the storm peaks identified in the buoy and model data did not match in time. Thereby, in order to make the validation process possible,

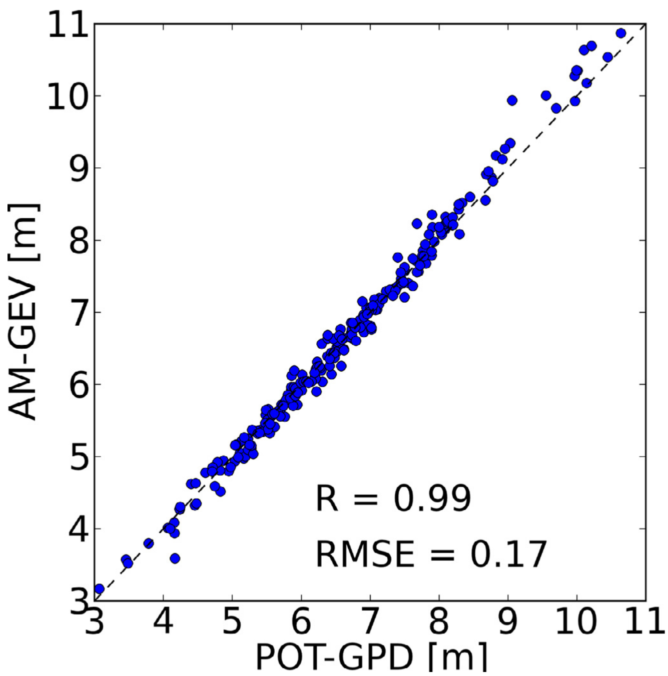

Fig. 9. Quantile-Quantile comparison of Hs return values for 100-year return period estimated using both the Annual Maxima-Generalised Extreme Value Distribution (AM-GEV) and Peaks-Over-Threshold-Generalised Pareto Distribution (POT-GPD) approaches. Return values were estimated at the model grid points on the 50 m isobath. *R* and *RMSE* stand for Pearson's correlation coefficient and root-mean-square error, respectively.

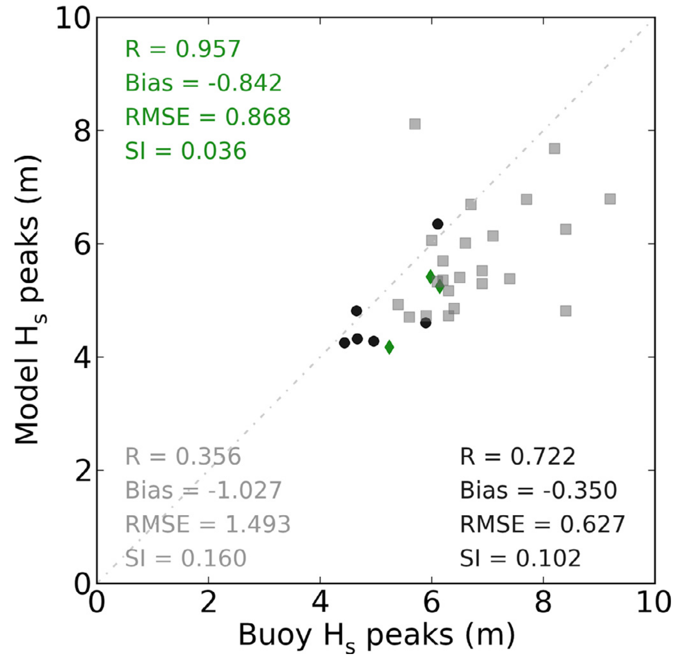

Fig. 11. Validation of modelled significant wave height peaks during overlapping periods with buoy data for Baring Head (black circles), Banks Peninsula (green diamonds) and Maui (grey squares). Basic statistics (Pearson's correlation coefficient (*R*), bias in meters, root-mean-square error (*RMSE*) in meters, and scatter index (*SI*)) were calculated according to Durrant et al. (2009). (For interpretation of the references to colour in this figure legend, the reader is referred to the web version of this article.)

buoy and model peaks were considered as matching peaks when they occurred less than 24 h apart. Due to the relatively short overlapping periods in addition to gaps in the buoy data, only a few peaks could be used in the model validation. In total, 6 (black circles), 3 (green diamonds) and 23 (grey squares) matching peaks were identified at Baring Head, Banks Peninsula and Maui, respectively, during the approximately 3.5, 3 and 11 years of overlapping periods. Although calculating statistics from small samples (time series with only a few data points) is not ideal, and we do acknowledge the non-representativeness of these samples, they nevertheless provide an overview of how well the model reproduced the observed storm peaks during these specific overlapping periods. The validation was performed using the formulae of basic statistics (*R*, bias, *RMSE*, and scatter index (*SI*)) applied in Durrant et al. (2009). Not surprisingly, Hs peaks were generally underestimated by the model, as the bias values suggest (Fig. 11).

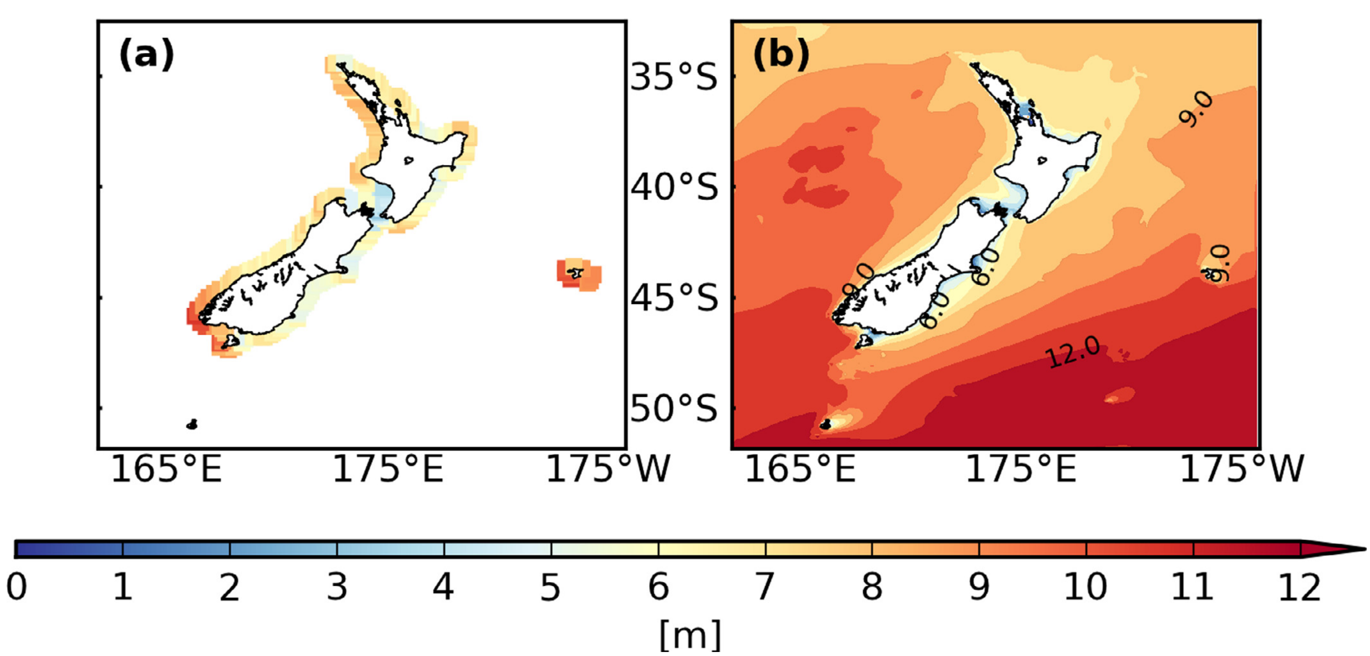

Fig. 10. Significant wave height return values for 100-year return period (a) estimated at the model grid points on the 50 m isobath using the Peaks-Over-Threshold-Generalised Pareto Distribution approach; (b) estimated for the whole regional domain using the Annual Maxima-Generalised Extreme Value Distribution approach.

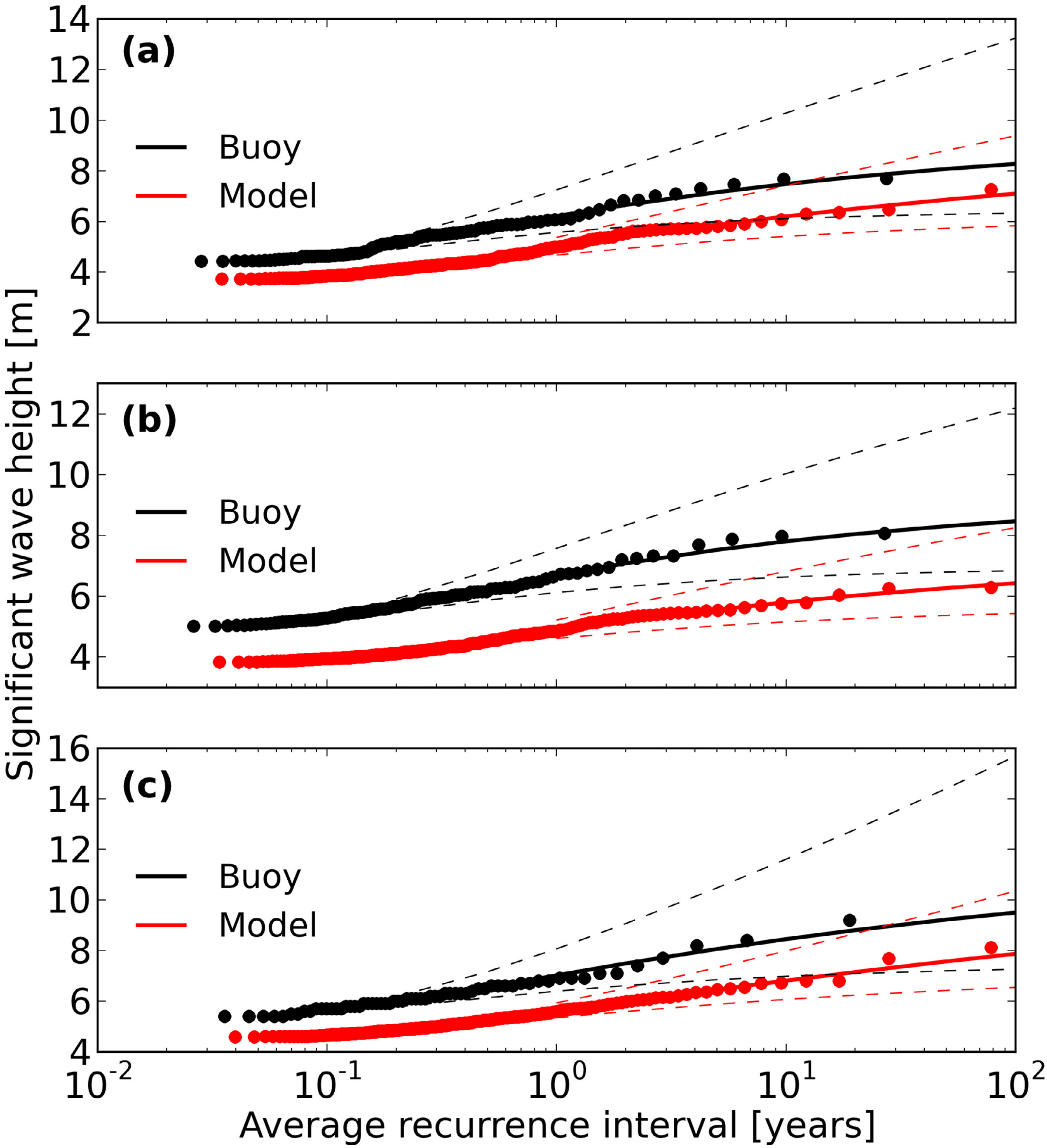

Fig. 12. Significant wave height return values (solid lines) estimated from the buoy (black) and model (red) data (Hs peaks from independent storms above the 99th percentile) for (a) Baring Head; (b) Banks Peninsula; (c) Maui. Dashed lines represent confidence intervals at the 95% level estimated from the asymptotic covariance matrix of the maximum likelihood estimators. Dots represent the data plotted in their Gringorten plotting positions (Gringorten, 1963). (For interpretation of the references to colour in this figure legend, the reader is referred to the web version of this article.)

Additionally, the model did not present any clear trends regarding the magnitude of the underestimates as the Hs peaks increased. The different sample sizes preclude comparing statistics between these three buoy sites.

As expected, Hs return values estimated from the model data underestimated the ones calculated from the buoy data (Fig. 12) by up to 24.12% for the 100-year return period (at Banks Peninsula). For the same return period, an average across the three sites indicates a bias correction of 18.58% for the model data. However, as briefly discussed in Section 2, calibration of the model data based on limited buoy records is not recommended, especially when dealing with extreme events. Cavaleri (2009) lists several reasons

Please cite this article as: V.A. Godoi et al., Extreme waves in New Zealand waters, Ocean Modelling (2017), http://dx.doi.org/10.1016/j.ocemod.2017.08.004

why storm peaks are not properly captured by wave simulations. In addition to these, the hindcast was carried out using wind fields with relatively coarse space-time resolution and also adopting a source term package (Tolman and Chalikov, 1996) that results in underestimation of the energy input during intense storm conditions dominated by young wind-sea (Ardhuin et al., 2007). Moreover, Hs return values were computed from datasets spanning different periods of time. Lastly, as revealed by the trend analysis (Fig. 8), trends in extreme Hs and in the number of extreme events have been detected, especially on the east coast, where two of the buoys are located. Despite all the issues and disregarding the estimates computed for Banks Peninsula, one notes that the 100-year estimates calculated from both datasets indicate a reasonable match when the confidence intervals are taken into account. The largest 100-year Hs return value calculated from the most reliable set of buoy measurements used in this work (buoy data from Maui) was 9.50 m (Fig. 12c). Considering the error estimates, this value increases to approximately 16 m. This dataset was collected near the west coast of the North Island (Fig. 1), whereas the largest waves occur in southern New Zealand. Therefore, for design purposes, it is reasonable to expect waves around New Zealand with Hs larger than 16 m, especially along the southwestern coast.

5. Discussion

Although it is beyond the scope of the present work to investigate the relationship between extreme wave events and climate patterns, some evidence of this connection is documented here and motivates future work.

The IAV of extreme Hs found in the central north coast of New Zealand (Fig. 7b) is likely associated with La Niña episodes. Larger waves on the north coast have been reported during La Niña conditions (Godoi et al., 2016; Gorman et al., 2003a) as a consequence of stronger northeasterly winds (Gordon, 1986). Furthermore, tropical cyclones tend to be formed closer to the country during La Niña episodes (Revell and Goulter, 1986), and this might favour extreme waves, which in turn tend to be generated by local storms (Young et al., 2011). A strong association between local storms and extreme waves was demonstrated by Young et al. (2011) through similar positive trends in wind speed and wave height for 99th percentile conditions. La Niña-like effects can be caused by at least three climate patterns: the El Niño-Southern Oscillation (ENSO), the Pacific Decadal Oscillation (PDO), and the Indian Ocean Dipole (IOD) (Godoi et al., 2016). Correlations between ENSO and PDO indices have been verified (Godoi et al., 2016; Mantua et al., 1997), suggesting that the PDO can influence the ENSO phases (La Niña and El Niño). The IOD can be externally triggered by the ENSO (Schott et al., 2009), and indirect effects of the first can take place through the second owing to the correlation between these two modes. The opposite is also true, meaning that the IOD is able to promote conditions that facilitate the formation of the ENSO (Izumo et al., 2010).

The negative trends observed in part of the west coast of the South Island (Fig. 8a and b) contrast the increase in intensity of cyclones in the Tasman Sea reported by Simmonds and Keay (2000). One would expect stronger cyclones to be associated with an increasing trend in extreme Hs. On the other hand, the negative trend on the west coast found here might be related to a poleward shift of extratropical cyclone storm tracks (Gillett and Thompson, 2003), which is more likely to favour southerly waves (those that impact the east coast) than westerly ones. This poleward shift, consistent with the trend for a more positive SAM (Marshall, 2003), results in a southward displacement of wave generation zones. As a consequence, waves generated more to the south affect the east coast more than the waters immediately adjacent to the west coast, due to their propagation in great circles. Godoi et al. (2016) showed that, in terms of mean conditions, significant wave height (Hs) was positively correlated with the SAM on the south and east coasts of the country during the period 1958–2001, whereas a negative correlation was found on the waters immediately adjacent to the west coast, with both correlations being statistically significant. A similar pattern was found for more extreme conditions (top 10% Hs), although correlations with the SAM in the waters immediately adjacent to the South Island were not statistically significant. Moreover, decreasing/increasing trends in westerly/southwesterly waves on the west coast of New Zealand have been documented, in addition to increasing/decreasing trends in southerly/southeasterly waves on the east coast (Hemer et al., 2010). Using satellite data, Young et al. (2011) noted statistically significant positive trends in extreme Hs in the region around New Zealand. Nevertheless, the period (1985–2008) considered in their analysis was shorter than and different from ours, and they used a considerably coarser dataset than the ones employed here. It should be clear that climate trends identified in reanalysis datasets can be greatly influenced by temporal changes in the quality and quantity of the data assimilated into the model. Such changes were also introduced to the fields of the ERA-40 reanalysis (Bengtsson et al., 2004; Uppala et al., 2005) used to force the 45WH. Nonetheless, some of the trends detected here are in agreement with trends reported by authors (e.g., Marshall, 2003; Young et al., 2011) who used data from meteorological stations and satellite altimeters. Furthermore, Marshall (2003) stated that ERA-40 can be used with high confidence, at least as far back as 1973, to examine the recent trend in the SAM, whose main signature occurs in the high latitudes of the Southern Hemisphere. High and mid-latitudes comprise the main wave generation zones responsible for the formation of the waves that consistently impact on the New Zealand coastline.

6. Conclusion

Based on 44 years (1958–2001) of a high resolution wave hindcast, an extreme wave climatology and extreme value estimates were established for New Zealand waters. Monthly and seasonal climatologies, mean annual and interannual variabilities, and trend analyses compose the extreme wave climatology. Extreme predictions were carried out employing two different approaches, the POT-GPD and AM-GEV. Their results were compared, and the POT-GPD estimates were in addition compared to estimates conducted from buoy data at three specific locations.

The extreme Hs and mean Hs (Godoi et al., 2016) spatial patterns are similar in both offshore and coastal areas, with the roughest seas found in southern New Zealand and calmer conditions observed in regions sheltered from southwesterly swells. This was observed not only in climatological parameters, but also in estimates of Hs return values. Nevertheless, some differences, such as high energetic waves on the northwestern coast in January as well as the intensity of events, stress the importance of exploring extreme and mean conditions separately.

The time of the year and coastline exposure to generating regions are key factors in determining the frequency of extreme events. Except for the north coast, New Zealand was hit by a large number of events in May, while they were least frequent in January and February. Extreme Hs had little seasonal variation, but closely-spaced extreme conditions were more/less frequent in winter/summer around the whole country. Regions where locally-generated storms control the extreme wave climate presented greatest MAV. Given that the IAV of mean wave conditions is correlated with La Niña-like effects on the north coast, which might have different sources (ENSO, IOD and PDO), and with the SAM on the east coast, it is likely that the IAV of extreme Hs is also driven by these oscillations. Statistically significant negative trends in extreme Hs were detected in parts of the west coast of the South Island, indicating a possible relationship with the poleward shift of extratropical cyclone storm tracks (Gillett and Thompson, 2003). Increasing trends detected in parts of the east coast of the same island suggest an association with positive trends in the SAM (Hemer, 2010; Marshall, 2003). The latter also seems to be related to the increasing frequency of extreme waves on the east and south coasts of New Zealand. These assumptions regarding relationships between climate patterns and the extreme wave climate around New Zealand deserve further investigation.

Analogous results were obtained by the POT-GPD and AM-GEV methods when comparing 100-year Hs return values, although the AM-GEV method estimated slightly larger waves at the highest quantiles. Estimates computed from the model data were lower than those calculated from the buoy data for Baring Head, Banks Peninsula and Maui as a result of several factors. These include model inputs with coarse space-time resolution, selection of a source term package (Tolman and Chalikov, 1996) that results in underestimation of the energy input during intense storm conditions dominated by young wind-sea (Ardhuin et al., 2007), and datasets spanning different periods of time.

As stated by Mathiesen et al. (1994), water level statistics become important in estimating extreme waves at shallow water locations, and these were not considered here. Several factors can potentially threaten coastal areas in New Zealand, such as land subsidence due to groundwater withdrawal, sea-level rise (Bell et al., 2000; Hannah, 2004), and mangrove forests degradation or removal (although relatively uncommon in New Zealand, mangrove forests degradation and/or removal have occurred in isolated episodes – Morrisey et al., 2007; Stokes and Harris, 2015). These combined with extreme wave events result in an increased risk for the expanding coastal population of the country and its associated industrial, residential and tourism developments. Therefore, the results presented here may contribute significantly to safety and economic strategies in addition to providing relevant information for climatological applications.

Acknowledgments

This research has been funded by the Coordenação de Aperfeiçoamento de Pessoal de Nível Superior (CAPES) [grant number BEX9551/13-1]. The 45-year wave hindcast was conducted under the scope of the "Wave and storm-surge projections" (WASP) project, funded through the New Zealand Ministry of Science and Innovation [contract C01X0806]. KRB, SAS and RMG are funded by Hazards Platform contract C05X0907. The first author is thankful to Ricardo M. Campos for pertinent discussions on extreme value analysis. Lastly, the authors thank the reviewers for providing insightful comments, which led to major improvements in the work.

References

Alves, J.H.G.M., Young, I.R., 2003. On estimating extreme wave heights using combined Geosat, Topex/Poseidon and ERS-1 altimeter data. Appl. Ocean Res. 25, 167–186. doi:10.1016/j.apor.2004.01.002.
Ardhuin, F., Herbers, T.H.C., van Vledder, G.P., Watts, K.P., Jessen, R., Graber, H.C., 2007. Swell and slanting fetch effects on wind wave growth. J. Phys. Oceanogr. 37, 908–931. doi:10.1175/JPO3039.1.
Ardhuin, F., Rogers, E., Babanin, A.V., Filipot, J.-F., Magne, R., Roland, A., van der Westhuysen, A., Queffeulou, P., Lefevre, J.-M., Aouf, L., Collard, F., 2010. Semiempirical dissipation source functions for ocean waves. Part I: definition, calibration, and validation. J. Phys. Oceanogr. 40 (9), 1917–1941. doi:10.1175/2010JPO4324.1.
Bell, R.G., Goring, D.G., de Lange, W.P., 2000. Sea-level change and storm surges in the context of climate change. Inst. Prof. Eng. N. Z. (IPENZ) Trans. 27 (1), 1–10.
Bengtsson, L., Hagemann, S., Hodges, K.I., 2004. Can climate trends be calculated from reanalysis data? J. Geophys. Res. 109, D11111. doi:10.1029/2004JD004536.
Bryan, K.R., Kench, P.S., Hart, D.E., 2008. Multi-decadal coastal change in New Zealand: Evidence, mechanisms and implications. N. Z. Geogr. 64 (2), 117–128. doi:10.1111/j.1745-7939.2008.00135.x.
Caires, S., Sterl, A., 2003. Validation of ocean wind and wave data using triple collocation. J. Geophys. Res. 108 (C3). doi:10.1029/2002JC001491.
Caires, S., Sterl, A., Bidlot, J.-R., Graham, N., Swail, V., 2004. Intercomparison of different wind-wave reanalyses. J. Clim. 17 (10), 1893–1913. doi:10.1175/1520-0442(2004)017⟨1893:IODWR⟩2.0.CO;2.
Caires, S., Sterl, A., 2005. 100-Year return value estimates for ocean wind speed and significant wave height from the ERA-40 data. J. Clim. 18, 1032–1048. doi:10.1175/JCLI-3312.1.
Carter, D.J.T., Draper, L., 1988. Has the north-east Atlantic become rougher? Nature 332, 494. doi:10.1038/332494a0.
Cavaleri, L., 2009. Wave modeling – missing the peaks. J. Phys. Oceanogr. 39, 2757–2778. doi:10.1175/2009JPO4067.1.
Chawla, A., Spindler, D.M., Tolman, H.L., 2013. Validation of a thirty year wave hindcast using the Climate Forecast System Reanalysis winds. Ocean Modell. 70, 189–206. doi:10.1016/j.ocemod.2012.07.005.
Coles, S.G., 2001. An Introduction to Statistical Modelling of Extreme Values. Springer, London doi:10.1007/978-1-4471-3675-0.
Durrant, T.H., Greenslade, D.J.M., Simmonds, I., 2009. Validation of Jason-1 and Envisat remotely sensed wave heights. J. Atmos. Ocean. Tech. 26, 123–134. doi:10.1175/2008JTECHO598.1.
Ferreira, J.A., Guedes Soares, C., 1998. An application of the Peaks Over Threshold method to predict extremes of significant wave height. J. Offshore Mech. Arct. Eng. 120 (3), 165–176. doi:10.1115/1.2829537.
Gillett, N.P., Thompson, D.W.J., 2003. Simulation of recent Southern Hemisphere climate change. Science 302 (5643), 273–275. doi:10.1126/science.1087440.
Godoi, V.A., Bryan, K.R., Gorman, R.M., 2016. Regional influence of climate patterns on the wave climate of the southwestern pacific: the New Zealand region. J. Geophys. Res. 121 (6), 4056–4076. doi:10.1002/2015JC011572.
Gordon, N.D., 1986. The southern oscillation and New Zealand weather. Mon. Weather Rev. 14, 371–387. doi:10.1175/1520-0493(1986)114⟨0371:TSOANZ⟩2.0.CO;2.
Gorman, R.M., Bryan, K.R., Laing, A.K., 2003a. Wave hindcast for the New Zealand region: nearshore validation and coastal wave climate. N.Z. J. Mar. Freshwater Res. 37 (3), 567–588. doi:10.1080/00288330.2003.9517190.
Gorman, R.M., Bryan, K.R., Laing, A.K., 2003b. Wave hindcast for the New Zealand region: deep-water wave climate. N.Z. J. Mar. Freshwater Res. 37 (3), 589–612. doi:10.1080/00288330.2003.9517191.
Gorman, R.M., Bell, R.G., Lane, E.M., Gillibrand, P.A., Stephens, S.A., 2010. New Zealand wave climate – simulating the past and future. Paper Presented at New Zealand Coastal Society Annual Conference, 17–19 Nov. New Zealand Coastal Society, Whitianga, New Zealand.
Gringorten, I.I., 1963. A plotting rule for extreme probability paper. J. Geophys. Res. 68 (3), 813–814. doi:10.1029/JZ068i003p00813.
Guedes Soares, C., Scotto, M.G., 2004. Application of the r largest-order statistics for long-term predictions of significant wave height. Coastal Eng. 51, 387–394. doi:10.1016/j.coastaleng.2004.04.003.
Hannah, J., 2004. An updated analysis of long-term sea level change in New Zealand. Geophys. Res. Lett. 31, L03307. doi:10.1029/2003GL019166.
Hannah, J., Bell, R.G., 2012. Regional sea level trends in New Zealand. J. Geophys. Res. 117, C01004. doi:10.1029/2011JC007591.
Harley, M.D., Turner, I.L., Short, A.D., Ranasinghe, R., 2010. Interannual variability and controls of the Sydney wave climate. Int. J. Climatol. 30, 1322–1335. doi:10.1002/joc.1962.
Hartigan, J.A., Wong, M.A., 1979. Algorithm AS 136: A K-Means clustering algorithm. J. R. Stat. Soc. Ser. C. 28 (1), 100–108. doi:10.2307/2346830.
Hauer, ME., Evans, J.M, Mishra, D.R., 2016. Millions projected to be at risk from sea-level rise in the continental United States. Nat. Clim. Change. 1–5. doi:10.1038/nclimate2961.
Hemer, M.A., 2010. Historical trends in Southern Ocean storminess: long-term variability of extreme wave heights at Cape Sorell, Tasmania. Geophys. Res. Lett. 37 (18), L18601. doi:10.1029/2010GL044595.
Hemer, M.A., Church, J.A., Hunter, J.R., 2010. Variability and trends in the directional wave climate of the Southern Hemisphere. Int. J. Climatol. 30 (4), 475–491. doi:10.1002/joc.1900.
Hemer, M.A., Zieger, S., Durrant, T., O'Grady, J., Hoeke, R.K., McInnes, K.L., Rosebrock, U., 2016. A revised assessment of Australia's national wave energy resource. Renewable Energy. doi:10.1016/j.renene.2016.08.039.
Holthuijsen, L.H., 2007. Waves in Oceanic and Coastal Waters. Cambridge University Press, New York doi:10.1017/CBO9780511618536.
Horrillo-Caraballo, J.M., Pan, S., Reeve, D.E., Simmonds, D., Greaves, D., Fox, A., 2012. Modelling extreme wave events (present and future scenarios) in southwest England. In: Paper presented at Proceedings of 33rd Conference on Coastal Engineering, Santander, Spain, 1–6 July 2012. Published in Lynett, Patrick and Smith, Jane McKee eds, Coastal Engineering 2012, Proceedings of 33rd Annual Conference, 33. Coastal Engineering Research Council doi:10.9753/icce.v33.waves.46.
Izaguirre, C., Méndez, F.J., Menéndez, M., Losada, I.J., 2011. Global extreme wave height variability based on satellite data. Geophys. Res. Lett. 38, L10607. doi:10.1029/2011GL047302.
Izumo, T., Vialard, J., Lengaigne, M., Montegut, C.B., Behera, S.K., Luo, J., Cravatte, S., Masson, S., Yamagata, T., 2010. Influence of the state of the Indian Ocean Dipole on the following year's El Niño. Nat. Geosci. 3, 168–172. doi:10.1038/ngeo760.
Kanungo, T., Mount, D.M., Netanyahu, N.S., Piatko, C.D., Silverman, R., Wu, A.Y., 2002. An efficient K-Means clustering algorithm: analysis and implementation. IEEE Trans. Pattern Anal. Mach. Intell. 24 (7), 881–892. doi:10.1109/TPAMI.2002.1017616.

Kendall, M.G., 1955. Rank Correlation Methods, second ed. Charles Griffin and Company, London.
Kushner, P.J., Held, I.M., Delworth, T.L., 2001. Southern Hemisphere atmospheric circulation response to global warming. J. Clim. 14 (10), 2238–2249. doi:10.1175/1520-0442(2001)014⟨0001:SHACRT⟩2.0.CO;2.
Laing, A.K., 2000. New Zealand wave climate from satellite observations. N. Z. J. Mar. Freshwater Res. 34 (4), 727–744. doi:10.1080/00288330.2000.9516973.
Lavergne, C., Palter, J.B., Galbraith, E.D., Bernardello, R., Marinov, I., 2014. Cessation of deep convection in the open Southern Ocean under anthropogenic climate change. Nat. Clim. Change 4, 278–282. doi:10.1038/nclimate2132.
Mann, H.B., 1945. Nonparametric tests against trend. Econometrica 13 (3), 245–259. doi:10.2307/1907187.
Mantua, N.J., Hare, S.R., Zhang, Y., Wallace, J.M., Francis, R.C., 1997. A Pacific interdecadal climate oscillation with impacts on salmon production. Bull. Am. Meteorol. Soc. 78 (6), 1069–1079. doi:10.1175/1520-0477(1997)078⟨1069:APICOW⟩2.0.CO;2.
Marshall, G.J., 2003. Trends in the Southern Annular Mode from observations and reanalyses. J. Clim. 16 (24), 4134–4143. doi:10.1175/1520-0442(2003)016⟨4134:TITSAM⟩2.0.CO;2.
Mathiesen, M., Goda, Y., Hawkes, P.J., Mansard, E., Martín, M.J., Peltier, E., Thompson, E.F., Vledder, G.V., 1994. Recommended practice for extreme wave analysis. J. Hydraul. Res. 32 (6), 803–814. doi:10.1080/00221689409498691.
Mazas, F., Hamm, L., 2011. A multi-distribution approach to POT methods for determining extreme wave heights. Coastal Eng. 58, 385–394. doi:10.1016/j.coastaleng.2010.12.003.
Méndez, F.J., Menéndez, M., Luceño, A., Losada, I.J., 2006. Estimation of the long-term variability of extreme significant wave height using a time-dependent Peak Over Threshold (POT) model. J. Geophys. Res. 111, C07024. doi:10.1029/2005JC003344.
Méndez, F.J., Menéndez, M., Luceño, A., Medina, R., Graham, N.E., 2008. Seasonality and duration in extreme value distributions of significant wave height. Ocean Eng. 35, 131–138. doi:10.1016/j.oceaneng.2007.07.012.
Menéndez, M., Méndez, F.J., Izaguirre, C., Luceño, A., Losada, I.J., 2009. The influence of seasonality on estimating return values of significant wave height. Coastal Eng. 56, 211–219. doi:10.1016/j.coastaleng.2008.07.004.
Moeini, M.H., Etemad-Shahidi, A., Chegini, V., 2010. Wave modeling and extreme value analysis off the northern coast of the Persian Gulf. Appl. Ocean Res. 32, 209–218. doi:10.1016/j.apor.2009.10.005.
Morrisey, D., Beard, C., Morrison, M., Craggs, R., Lowe, M., 2007. The New Zealand Mangrove: Review of the Current State of Knowledge. Auckland Regional Council Technical Publication Number 325.
Neelamani, S., Al-Salem, K., Rakha, K., 2007. Extreme waves for Kuwaiti territorial waters. Ocean Eng. 34, 1469–1504. doi:10.1016/j.oceaneng.2006.08.013.
Neumann, C.J., 1993. “Global overview” – Chapter 1, Global guide to tropical cyclone forecasting. WMO/TD-No560. Report No. TCP-31. World Meteorological Organization, Geneva, Switzerland.
Pickrill, R.A., Mitchell, J.S., 1979. Ocean wave characteristics around New Zealand. N.Z. J. Mar. Freshwater Res. 13 (4), 501–520. doi:10.1080/00288330.1979.9515827.
Revell, C.G., Goulter, S.W., 1986. South Pacific tropical cyclones and the Southern Oscillation. Mon. Weather Rev. 114 (6), 1138–1145. doi:10.1175/1520-0493(1986)114⟨1138:SPTCAT⟩2.0.CO;2.
Ruggiero, P., Komar, P.D., Allan, J.C., 2010. Increasing wave heights and extreme value projections: the wave climate of the U.S. Pacific Northwest. Coastal Eng. 57, 539–552. doi:10.1016/j.coastaleng.2009.12.005.
Schott, F.A., Xie, S., McCreary, J.P., 2009. Indian Ocean circulation and climate variability. Rev. Geophys. 47, RG1002. doi:10.1029/2007RG000245.
Sen, P.K., 1968. Estimates of the regression coefficient based on Kendall's Tau. J. Amer. Statist. Assoc. 63 (324), 1379–1389. doi:10.1080/01621459.1968.10480934.
Simmonds, I., Keay, K., 2000. Variability of Southern Hemisphere extratropical cyclone behavior, 1958–97. J. Clim. 13 (2), 550–561. doi:10.1175/15200442(2000)013⟨0550:VOSHEC⟩2.0.CO;2.
Stephens, S.A., Gorman, R.M., 2006. Extreme wave predictions around New Zealand from hindcast data. N.Z. J. Mar. Freshwater Res. 40 (3), 399–411. doi:10.1080/00288330.2006.9517431.
Stokes, D.J, Harris, R.J., 2015. Sediment properties and surface erodibility following a large-scale mangrove (Avicennia marina) removal. Continental Shelf Res. 107, 1–10. doi:10.1016/j.csr.2015.07.011.
Stopa, J.E., Ardhuin, F., Babanin, A., Zieger, S., 2016. Comparison and validation of physical wave parameterizations in spectral wave models. Ocean Modell. 130, 2–17. doi:10.1016/j.ocemod.2015.09.003.
Stopa, J.E., Cheung, K.F., Tolman, H.L., Chawla, A., 2013. Patterns and cycles in the climate forecast system reanalysis wind and wave data. Ocean Modell. 70, 207–220. doi:10.1016/j.ocemod.2012.10.005.
Swail, V.R., Cardone, V.J., Ferguson, M., Gummer, D.J., Harris, E.L., Orelup, E.A., Cox, A.T., 2006. The MSC50 wind and wave reanalysis. In: Proc. 9th International Workshop On Wave Hindcast and Forecasting, September 25–29. Victoria, B.C. Canada.
Theil, H., 1950. A rank-invariant method of linear and polynomial regression analysis. In: Proceedings of the Royal Netherlands Academy of Sciences. 53, Part I: 386-392, Part II: 521-525 and Part III: 1397-1412.
Tolman, H.L. User manual and system documentation of WAVEWATCH III version 3.14 NOAA/NWS/NCEP/MMAB Tech. Note 276, 194 pp + Appendices, NOAA, Camp Springs, Md. [Available at http://polar.ncep.noaa.gov/waves/wavewatch/wavewatch.shtml].
Tolman, H.L., Chalikov, D.V., 1996. Source terms in a third-generation wind-wave model. J. Phys. Oceanogr. 26 (11), 2497–2518. doi:10.1175/1520-0485(1996)026⟨2497:STIATG⟩2.0.CO;2.
Uppala, S.M., Kallberg, P.W., Simmons, A.J., Andrae, U., Bechtold, V.D.C., Fiorino, M., Gibson, J.K., Haseler, J., Hernandez, A., Kelly, G.A., Li, X., Onogi, K., Saarinen, S., Sokka, N., Allan, R.P., Andersson, E., Arpe, K., Balmaseda, M.A., Beljaars, A.C.M., Berg, L.V.D., Bidlot, J., Bormann, N., Caires, S., Chevallier, F., Dethof, A., Dragosavac, M., Fisher, M., Fuentes, M., Hagemann, S., Hólm, E., Hoskins, B.J., Isaksen, L., Janssen, P.A.E.M., Jenne, R., Mcnally, A.P., Mahfouf, J.-F., Morcrette, J.-J., Rayner, N.A., Saunders, R.W., Simon, P., Sterl, A., Trenberth, K.E., Untch, A., Vasiljevic, D., Viterbo, P., Woollen, J., 2005. The ERA-40 re-analysis. Quart. J. Roy. Meteorol. Soc. 131 (612), 2961–3012. doi:10.1256/qj.04.176.
Vinoth, J., Young, I.R., 2011. Global estimates of extreme wind speed and wave height. J. Clim. 24, 1647–1665. doi:10.1175/2010JCLI3680.1.
World Bank Group, 2016. Global Economic Prospects, January 2016: Spillovers amid Weak Growth. World Bank, Washington, D. C. doi:10.1596/978-1-4648-0675-9.
Young, I.R., Zieger, S., Babanin, A.V., 2011. Global trends in wind speed and wave height. Science 332, 451–455. doi:10.1126/science.1197219.
Young, I.R., Vinoth, J., Zieger, S., Babanin, A.V., 2012. Investigation on trends in extreme value wave height and wind speed. J. Geophys. Res. 117, C00J06. doi:10.1029/2011JC007753.